Dual-Band Planar Plasmonic Unidirectional Launching in a Semiannular Apertures Array

Shan Huang,*,†,‡ Chun-Yuan Wang,† Hung-Ying Chen,† Meng-Hsien Lin,† Yu-Jung Lu,† and Shangjr Gwo*,†

†Department of Physics, National Tsing-Hua University, Hsinchu 30013, Taiwan

‡Jiangxi Key Laboratory of Nanomaterials and Sensors, Jiangxi Key Laboratory of Photoelectronics and Telecommunication, School of Physics, Communication and Electronics, Jiangxi Normal University, Nanchang 330022, Jiangxi, China

Ⓢ *Supporting Information*

ABSTRACT: Multiple-band, frequency-adjustable unidirectional launching of planar surface plasmons is of great concern in plasmonic devices and circuits. We have designed and demonstrated a novel dual-band planar unidirectional surface plasmon polaritons (SPPs) launcher with narrow bandwidth (~5 nm) and large band gap (~50 nm) using a semiannular apertures array milled in a gold film. Symmetry breaking of the semiannular aperture brings significant advantages for the unidirectional launching, based on the excited asymmetrically distributed cylindrical surface plasmon resonance modes. During the unidirectional launching, the individual semiannular apertures function as unidirectional quasi-point SPP sources, and the grating coherently stacking amplitude of unidirectional SPPs functions as an amplifier. By controlling the semiannular aperture size, we achieved large range modulations of wavelengths beyond 60 nm for both bands. This efficient unidirectional launching is experimentally demonstrated for 632 nm, showing good agreement with numerical results.

KEYWORDS: unidirectional launching, surface plasmon polaritons, cylindrical surface plasmons, semiannular aperture
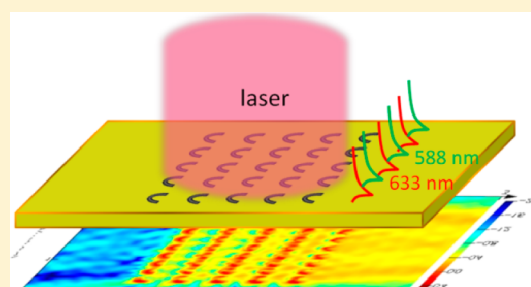
Plasmonic nanostructures have attracted much research attention because of their outstanding ability in manipulating light at nanoscale. Taking advantage of the strong dependence of the optical response on the composition and geometry of the structure, numerous plasmonic nanostructures have been designed to realize novel optical phenomena and can be applied in optical materials and devices, such as metamaterials,[1,2] sensors,[3−5] multiplexing plasmonic circuit elements,[6,7] and antennas.[8−10] Introducing symmetry breaking can result in the changes of the plasmonic mode excitation conditions, the spatial field and phase distribution in the plasmonic nanostrucutrue, which is considered as an important way to control the properties of the plasmonic nanostructure. Symmetry breaking nanostructures have been demonstrated to achieving magnetically excited mode,[11,12] Fano resonances,[13,14] and plasmonic focusing at nanoscale.[15] Recently, it was shown that symmetry breaking structure can induce strong directionality of the light emission.[16−19] In nanocups and semishells, the far-field scattering profile can be altered by controlling the perforation of the metallic shells.[18] And in a core−shell nanocavity, the spaser emission exclusively propagated along a specific direction, which is related to the appearance of new plasmon modes induced by the broken symmetry.[19]

On the other hand, achieving planar directional propagating of surface plasmon polaritons (SPPs) in metal surface is key for applications in integrated circuit. The unidirectional plasmonic launcher, which can be widely employed in coupling, filtering, polarization selecting, and switching, has been gradually developed in recent years.[20−25] Conventional approaches to achieving unidirectional launching (UL) involve the use of attenuated total reflection, which is very sensitive to the incident angle.[26] Recently, many different nanostructures are proposed to achieve unidirectional launching through the SPPs' destructive interference in nonlaunching directions and constructive interference in the launching direction, such as the period aperture grating,[27] the aperiodic groove arrays,[28,29] and the active controlled graphene-loaded reflective antenna pair structure.[30] In these reports, UL is related to the phase difference of the SPPs, so UL can only be realized in a particularly defined wavelength or band. Compared to a single band unidirectional launcher, the SPPs propagation direction can be controlled at several spectral positions simultaneously for a multiple band unidirectional launcher, which would be useful for multiple wavelength plasmonic circuits.

Here we use a semiannular apertures array milled in an Au film to achieving dual-band UL of planar SPPs propagating wave. Because of the symmetry breaking, cylindrical surface plasmon (CSP) modes with asymmetry mode profiles are excited in a semiannular aperture. Based on two different excited CSP modes, the dual-band UL has been realized in the

individual semiannular aperture. Compare to conventional periodic or aperiodic metallic gratings, where the UL is the collective effect of the gratings, each individual semiannular aperture in the proposed structure functions as a unidirectional quasi-point SPPs source, and the grating coherently stacking amplitude of unidirectional SPP functions as an amplifier. We experimentally observed the efficient UL of SPPs at visible wavelengths. A remarkable right-to-left UL extinction ratio of about 100:1 has been obtained by numerical simulations. Moreover, dual-band SPPs UL has been demonstrated with small bandwidth (~5 nm) and large band gap (~50 nm). The UL bands show sensitive dependence on the annular radius of each individual semiannular aperture, where a large range modulation of wavelength beyond 60 nm has been demonstrated for each band.

The periodic 10×5 semiannular apertures array with an area of ~3 μm $\times$ 5 μm is etched into an Au film using focused ion beam milling (FIB), as shown in Figure 1a. The film thickness
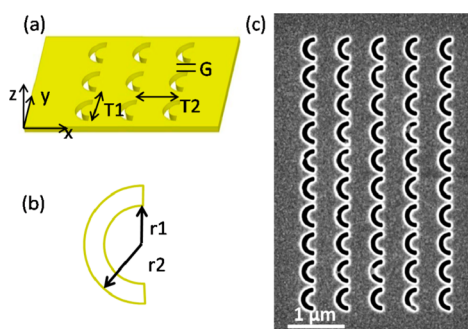
Figure 1. (a, b) Schematic of semiannular apertures milled in Au film. (c) Scanning electron microscopy image of semiannular apertures arrays. The film thickness is 100; r1 = 125 nm, r2 = 200 nm, T1 = 490 nm, and T2 = 600 nm.

is 100 nm. The periods in the y and x directions are T1 and T2, respectively. The gap between two neighboring paratactic semiannular apertures is G. Figure 1b shows the schematic structure of an individual semiannular aperture. r1 and r2 are the inner and outer radii of the aperture, respectively. Figure 1c shows a representative scanning electron microscopy (SEM) image of the fabricated semiannular apertures nanoarray, with r1 = 125 nm and r2 = 200 nm, and the periods of the array along y and x axes T1 = 490 nm and T2 = 600 nm. The corresponding gap between two paratactic semiannular apertures is G = 90 nm.

The structures are back-illuminated with a polarized 632 nm laser. At the air–gold interface, the launched SPPs propagating on the gold surface can leak radiation, which can be collected by a charge coupled device (CCD). Images of the distribution of leakage radiation are shown in Figure 2a,b, for polarization direction along the y and x axes, respectively. Under y-polarized illumination, the optical signal is only observed in the region of the semiannular apertures array, which is due to light transmitted directly through the apertures. The leak radiation of the propagating SPPs has not been observed at the two sides of the structures. When incident light polarization turn to x-direction, clearly seen in Figure 2b, the leakage radiation signal of propagating SPPs is detected at the right side of the structure. On the contrary, no signal is collected at the left side of the structure, which indicates an obvious UL phenomenon along the x-axis. One can see that the leakage radiation image
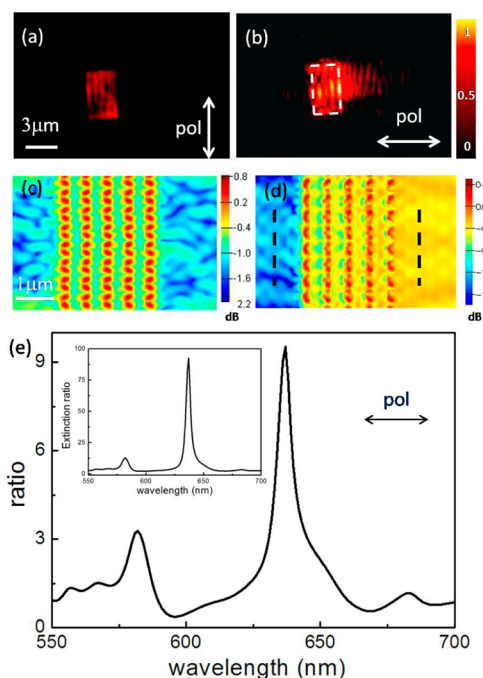
Figure 2. (a, b) CCD images of the semiannular array (r1 = 125 nm, r2 = 200 nm, T1 = 490 nm, T2 = 600 nm) under illumination from the back by y- and x-polarized light, respectively. (c, d) The FDTD simulated electric field magnitude distribution of the structure under y- (c) and x-polarized (d) illumination, corresponding to experimental observation. (e) The ratio of electric field amplitude in right side to left side. Inset: the extinction ratio spectra of the structure.

on the right side of the structure exhibits typical fringe patterns, which arise from the interference of the directly transmitted light with the leakage radiation of the SPPs. The intensity of the unidirectional launched SPPs decays exponentially along the propagating direction, with a propagation length of several microns, as shown in Figure S1 in Supporting Information.

In order to investigate the physical mechanism of this phenomenon, three-dimensional finite different time domain (FDTD) simulations are performed using commercial software (Lumerical Solution, Inc.). The gold dielectric constant is taken from the bulk value measured by Johnson and Christy.[31] The PML (perfectly matched layer) boundary condition is adopted to eliminate unwanted deviation. The environment is set as air with a refractive index n = 1. The electric-field magnitude distributions are simulated at the plane 10 nm above the film surface.

The simulated surface electric-field magnitude distributions matching the real array structures are in good agreement with the experimental observations, as shown in Figure 2c,d, which reveals an obvious SPPs UL phenomenon along the x-axis when under x-polarized incident light illumination. To quantify the UL intensity, the right-to-left ratio R is calculated, defined as the ratio of the electric field amplitude of the SPPs launching to the right (Ez+) to the amplitude launching to the left (Ez−). The power of the SPPs is in proportion to the squared perpendicular electric component $|Ez^2|$, thus, R^2 is proportional to the extinction ratio. We calculate the average electric amplitude along the black dotted lines as sketched in Figure 2d to represent the amplitude of the launched forward- and backward-propagating SPPs |Ez+| (right) and |Ez−| (left), where the black lines are 0.6 μm away from the boundaries of the structure.

Figure 2e show the dependence of the right-to-left ratio on the incident wavelength for the proposed semiannular apertures array. The spectrum has a peak at 633 nm, corresponding to observations. It should be noted that the extinction ratio R^2 reaches to ∼100 at 633 nm, as shown in the inset of Figure 2e, which is remarkable comparing with previously reported results, where the maximum unidirectional extinction ratio of ∼55 has been achieved for aperiodic metallic grooves.[29] In addition, the spectrum shows a secondary UL band with peak spectral position at 588 nm, with an extinction ratio of about 10. Both UL bands have narrow bandwidth of ∼5 nm, and the band gap between the two bands is very large (∼50 nm). In other words, the semiannular apertures array can provide dual–band UL with a narrow bandwidth (∼5 nm) and large band gap (∼50 nm) simultaneously, which have promising applications in multifrequency plasmonic circuits.

To explain the origin of the dual-band UL effect, we analyzed the resonance SPPs modes in an individual semiannular aperture. The near-field distributions at the spectral positions of the two UL bands are inspected. Figure 3a–d shows the
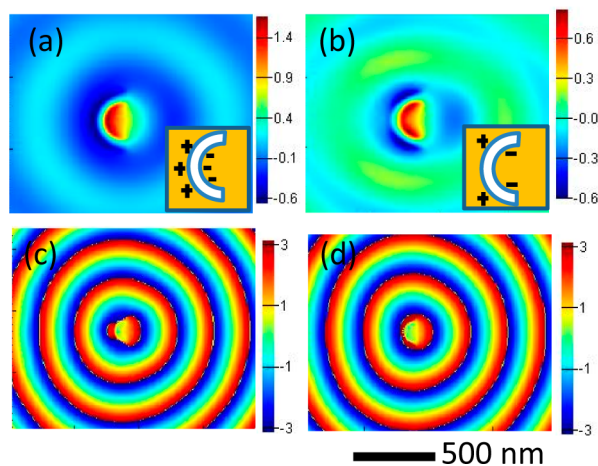
Figure 3. (a, b) FDTD simulated surface electric-field magnitude distribution of the cylindrical surface plasmon resonance modes HE_{11} (a) at 633 nm and HE_{21} (b) at 588 nm for an individual semiannular aperture, with r1 = 125 nm and r2 = 200 nm. The insets show the schematic charge distribution of the CSP modes. (c, d) Phase distribution of the corresponding CSP modes.

electric-field amplitude and phase distributions on the film surface of the two UL peaks at 588 and 633 nm, respectively. For the 633 nm peak, the electric field distribution of the resonance mode within the semiannular aperture indicates a dipole-like oscillation, as seen in Figure 3a. However, the field and phase distributions in the region outside the aperture, where the electric field of the resonant mode spreads outward radially and the phase distribution appears as concentric circles, are totally different from the typical dipole mode. For the resonance mode at 588 nm, the electric field distribution within the semiannular aperture shows a quadrupole-like oscillation, and the electric field and phase distribution outside the semiannular aperture is similar as the resonance mode at 633 nm, with concentric profile. Previous research shows that nanoscale coaxial annular apertures milled in metal film can support cylindrical surface plasmon (CSP) modes.[32] CSP existing in a nanoscale coaxial Au or Ag structure has been well investigated, which plays an important role in the extraordinary optical transmission phenomenon.[33−36] The CSP modes have a

Bessel field profile, the electric amplitude and phase of which have the same characteristics as radially polarized surface plasmon waves at the end faces of an annular aperture.[29] Thus, the features of the electric amplitude and phase distributions shown in Figure 3 indicate that the CSP modes are still retained in the semiannular apertures. The schematic charge distributions (Figure 3a,b, insets) imply that the SPP resonance modes in semiannular aperture are HE_{11} CSP mode at 633 nm and HE_{21} CSP mode at 588 nm, respectively.

Compare with the symmetry distribution of the CSP modes in a full annular aperture, the cross section electrical field distribution of CSP modes in a semiannular aperture is asymmetric due to the symmetry breaking. It should be noted that the asymmetrically distributed CSP mode in an individual semiannular aperture is localized. To generate UL, the semiannular apertures array is adopted to excite the propagating SPPs through the interaction between the localized CSP modes. As shown in Figure S2, the electric field distribution of two closed semiannular apertures has been calculated, where the CSP modes in the neighboring apertures couple and excite propagating SPPs along the symmetry axis. And because of the asymmetry distribtution of the CSP modes, the propagating SPPs are unidirectionally launched. In the case of a one-dimensional semiannular aperture chain, the unidirectional excitation is more evident, as shown in Figure 4. The phase distributions of the unidirectional launched (the right side of the chain) propagating SPPs exhibit the plane wavefront characteristics. This phenomenon can be explained by the Huygens-Fresnel principle, where we suppose that the CSP mode in every semiannular aperture as a unidirectional quasi-point plasmonic source. According to the Huygens-Fresnel principle, the coherent superposition of a row of unidirectional point light source forms a unidirectional plane wave. Therefore, in semiannular aperture chain, every individual semiannular aperture considered as a unidirectional quasi-point plasmonic launcher with the same phase and excited the unidirectional propagating SPPs "plane" wave, radiating toward the right side of the semiannular aperture. Field distributions for two or more columns of semiannular aperture chains are provided in Figure S3, which show more evident UL of SPP "plane" waves. In addition, we have calculated the dependence of the UL on the incident angle, as shown in Figure S4. Limited by excitation condition of the CSP modes, the UL is very sensitive to the incident angle.

Next, we discuss the effects of modifying the geometry of the structure, including the radius, gap and period, on the UL bands. In a full annular apertures array, the resonant wavelength of the HE_{11} CSP mode increases indefinitely as $\lambda \sim r1/(r2 - r1)^{1/2}$ in the visible and IR wavelengths.[29] Here, the outer radius r2 is varied to tune the CSP modes and, thus, to tune the UL bands. Figure 4c shows the right-to-left ratio spectra of the semiannular array for different outer radii. As r2 increases from 120 to 160 nm (r1 = 100 nm, G = 40 nm), referring to an increase of period T1 from 280 to 360 nm, the HE_{11} CSP mode induced UL band is blue-shifted from 637 to 580 nm (Figure 4, black dotted line), with similar dependence on the outer radius as in the full annular aperture. Meanwhile, the intensity of the HE_{11} CSP induced UL is obviously modulated by r2, with a maximum ratio of nearly 100 when r2 = 130 nm. For the UL band related to the HE_{21} CSP mode, the UL peak shows red-shift with the peak wavelength increasing linearly from 579 to 630 nm with increasing of the outer radius r2. It is worth noting that the modulation spectral ranges of both bands are more
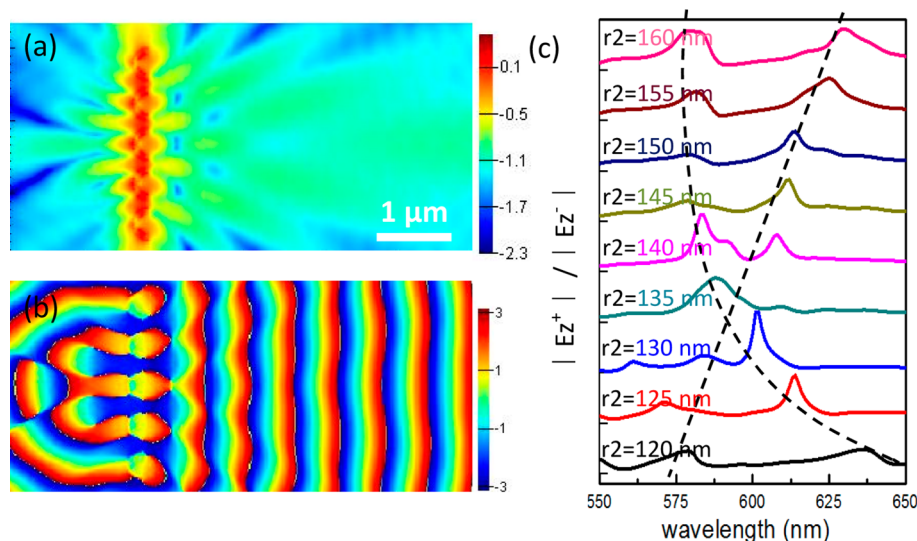
Figure 4. (a, b) FDTD-simulated surface electric-field magnitude distribution (a) and phase distribution (b) of the one-dimensional semiannular aperture chain. (c) The spectra of the right to left ratio of electric field amplitude in the semiannular apertures array with different outer radii r2 (from 120 to 160 nm). The gap G is unchanged at 40 nm, so T1 varies from 280 to 360 nm. The inner radius is r1 = 100 nm, and the period along the x-axis is T2 = 600 nm. Spectra are shifted upward for clarity.

than 50 nm, suggesting potential applications in integrated optoelectronic devices, as a complete, frequency-adjustable unidirectional SPPs launcher.

As discussed before, the interaction between the CSP modes of neighbor semiannular apertures excites the unidirectional propagating SPPs waves, thus, the gap between the two semiannular apertures G would play an important role in modulating the UL bands. Figure 5a shows the relationship between the right-to-left ratio spectra and G of the aperture array. As expected, the spectral positions of the two UL bands determined by the CSP resonance modes are unchanged, while the peak values of both bands are clearly modified. The maximum peak value of $R \sim 7$ occurs at $G = 30$ nm for the HE_{21} mode induced UL band (at a wavelength of 588 nm), and

the maximum peak value of $R \sim 9$ occurs at $G = 90$ nm for the HE_{11} mode band (at a wavelength of 633 nm). When the apertures are far apart, the interactions between the CSP modes weaken, and the amplitude of the excited propagating SPPs is decreased. When the distance between the apertures gets too small, the excitation condition of the CSP modes in each aperture is changed, which also influences the strength of the CSP modes. Thus, with an appropriate gap G, the CSP modes can achieve resonant oscillation, resulting in a maximum extinction ratio value.

In a full annular aperture array, the position of the resonance peak is hardly affected by periodicity. To see how the UL bands in semiannular aperture lattices are affected by the periodicity, in Figure 5b we examine the dependence of the right-to-left ratio R on the period T2. Figure 5b shows the right-to-left ratio spectra of the semiannular aperture array with increasing T2 from 530 to 640 nm, where the peak positions of the two UL bands remain at 588 and 633 nm, respectively. When T2 varied, both the peak values of the two bands show obvious modulation. The maximum peak value of $R \sim 4$ occurs at T2 = 550 nm for the HE_{21} band (at a wavelength of 588 nm), and the maximum peak value of $R \sim 10$ occurs at T1 = 600 nm for the HE_{11} band (at a wavelength of 633 nm). Using the standard dispersion relation for SPPs on a smooth metal−dielectric interface,[23] $k_{sp} = 2\pi/\lambda \sqrt{\varepsilon_m \varepsilon_d/(\varepsilon_m + \varepsilon_d)}$, with respective dielectric functions ε_m and ε_d, we can calculate that the SPP wavelengths of the corresponding incident free-space wavelengths 588/633 nm at the Au/air interface are 552/603 nm, where we adopt the gold dielectric constants of $-8.03 + 1.02i$ (at 588 nm) and $-10.92 + 0.81i$ (at 633 nm), respectively.[31] When the period T2 are close to the SPPs wavelengths 552/ 603 nm, the unidirectional SPPs waves excited in each semiannular aperture chain are in phase, and the constructive interference of the unidirectional SPP waves produce a maximum value of R. In other words, the periodicity of the aperture array along the x-axis functions as an amplifier if the spacing satisfies the constructive interference conditions. From Figure S5, we can clearly see that the unidirectional SPP waves
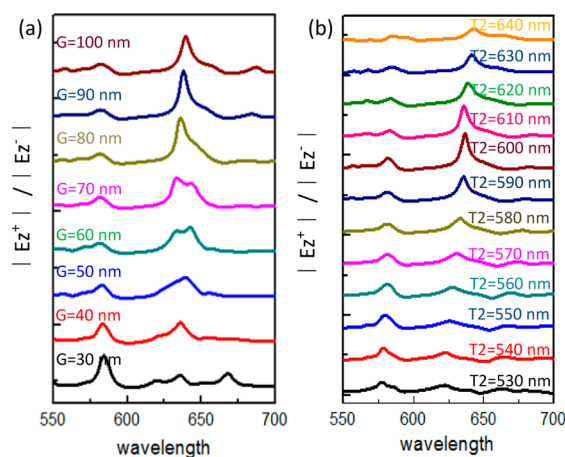
Figure 5. (a) Spectra of the right to left ratio of electric field amplitude in the semiannular apertures array with varying gaps between adjacent semiannular apertures G (from 30 to 100 nm). The inner radius is r1 = 125 nm, the outer radius is r2 = 200 nm, and T2 = 600 nm. (b) Spectra of the right to left ratio of electric field amplitude in the semiannular apertures array with various T2s (from 530 to 640 nm). The inner radius is r1 = 125 nm, the outer radius is r2 = 200 nm, and G = 90 nm. Spectra are shifted upward for clarity.

launched by each semiannular aperture chain stack up, leading to the extinction ratio R increasing step by step.

In this paper, we have detailed the dual-band unidirectional launcher structures consisting of a semiannular apertures array. UL at visible wavelengths was observed in our experiment. The results show good agreement with theoretical predictions. Two SPP UL bands, with a highest extinction ratio of about 100, and with a small bandwidth (~5 nm) and large band gap (~50 nm), are obtained using a semiannular apertures array, which are induced by the asymmetrically distributed CSP resonance modes. Every individual semiannular aperture can be considered as a unidirectional quasi-point SPP launcher, with SPP energy radiating toward the opening direction of the semiannular. The CSP modes depend sensitively on the annular radius, leading to a high tunability of the wavelength of the unidirectional bands. The tuning ranges of both bands exceed 60 nm, suggesting potential applications in integrated optoelectronic devices, as a complete adjustable frequency unidirectional SPP launcher. We have also demonstrated that the UL can be modified by changing the width of the gap between the apertures along the y-axis. If the period of the aperture array along the x-axis satisfies the constructive interference conditions, the UL SP waves stack coherently, leading to a maximum right-to-left ratio. In these cases, the periodicity of the aperture array along the x-axis functions as an amplifier. The proposed structure can be applied as multiple wavelength unidirectional launchers, and may find its applications in integrated optical circuits, nanoscaled laser sources, optical communications, and so on. In addition, our work contributes to our understanding of the viability of symmetry-breaking annular plasmonic structures

■ ASSOCIATED CONTENT

ⓈSupporting Information

The Supporting Information is available free of charge on the ACS Publications website at DOI: 10.1021/acsphotonics.5b00684.

> Experimentally measured optical intensity cross section distribution; the FDTD simulated electric field magnitude distribution of two closed semiannular apertures; the UL in different semiannular aperture chains; the spectra of the right to left ratio of electric field amplitude in the semiannular apertures array with different incident angle; the electric field cross section distribution of a five semiannular aperture chain structure (PDF).

■ AUTHOR INFORMATION

Corresponding Authors
*E-mail: huangshans1@163.com.
*E-mail: shangjr@hotmail.com.

Notes
The authors declare no competing financial interest.

■ ACKNOWLEDGMENTS

■ REFERENCES

(1) Ou, J. Y.; Plum, E.; Zhang, J. F.; Zheludev, N. I. An electromechanically reconfigurable plasmonic metamaterial operating in the near-infrared. *Nat. Nanotechnol.* **2013**, *8*, 252−255.

(2) Li, W.; Valentine, J. Metamaterial Perfect Absorber Based Hot Electron Photodetection. *Nano Lett.* **2014**, *14*, 3510−3514.

(3) Brolo, A. G. Plasmonics for future biosensors. *Nat. Photonics* **2012**, *6*, 709−713.

(4) Tong, L. M.; Wei, H.; Zhang, S. P.; Xu, H. X. Recent Advances in Plasmonic Sensors. *Sensors* **2014**, *14*, 7959−7973.

(5) Han, X. G.; Liu, Y. D.; Yin, Y. D. Colorimetric Stress Memory Sensor Based on Disassembly of Gold Nanoparticle Chains. *Nano Lett.* **2014**, *14*, 2466−2470.

(6) Li, L.; Li, T.; Wang, S. M.; Zhu, S. N.; Zhang, X. Broad Band Focusing and Demultiplexing of In-Plane Propagating Surface Plasmons. *Nano Lett.* **2011**, *11*, 4357−4361.

(7) Liu, J. S. Q.; Pala, R. A.; Afshinmanesh, F.; Cai, W. S.; Brongersma, M. L. A submicron plasmonic dichroic splitter. *Nat. Commun.* **2011**, *2*, 525.

(8) Abass, A.; Rodriguez, S. R. K.; Ako, T.; Aubert, T.; Verschuuren, M.; Van Thourhout, D.; Beeckman, J.; Hens, Z.; Rivas, J. G.; Maes, B. Active Liquid Crystal Tuning of Metallic Nanoantenna Enhanced Light Emission from Colloidal Quantum Dots. *Nano Lett.* **2014**, *14*, 5555−5560.

(9) Abb, M.; Wang, Y. D.; de Groot, C. H.; Muskens, O. L. Hotspot-mediated ultrafast nonlinear control of multifrequency plasmonic nanoantennas. *Nat. Commun.* **2014**, *5*, 4869.

(10) Shaltout, A.; Liu, J. J.; Shalaev, V. M.; Kildishev, A. V. Optically Active Metasurface with Non-Chiral Plasmonic Nanoantennas. *Nano Lett.* **2014**, *14*, 4426−4431.

(11) Linden, S.; Enkrich, C.; Wegener, M.; Zhou, J. F.; Koschny, T.; Soukoulis, C. M. Magnetic response of metamaterials at 100 terahertz. *Science* **2004**, *306*, 1351−1353.

(12) Enkrich, C.; Wegener, M.; Linden, S.; Burger, S.; Zschiedrich, L.; Schmidt, F.; Zhou, J. F.; Koschny, T.; Soukoulis, C. M. Magnetic metamaterials at telecommunication and visible frequencies. *Phys. Rev. Lett.* **2005**, *95*, 203901.

(13) Wallauer, J.; Walther, M. Fano line shape and phase reversal in a split-ring resonator based metamaterial. *Phys. Rev. B: Condens. Matter Mater. Phys.* **2013**, *88*, 195118.

(14) Zhang, Q.; Wen, X. L.; Li, G. Y.; Ruan, Q. F.; Wang, J. F.; Xiong, Q. H. Multiple Magnetic Mode-Based Fano Resonance in Split-Ring Resonator/Disk Nanocavities. *ACS Nano* **2013**, *7*, 11071−11078.

(15) Fang, Z. Y.; Peng, Q. A.; Song, W. T.; Hao, F. H.; Wang, J.; Nordlander, P.; Zhu, X. Plasmonic Focusing in Symmetry Broken Nanocorrals. *Nano Lett.* **2011**, *11*, 893−897.

(16) Luo, Y.; Lei, D. Y.; Maier, S. A.; Pendry, J. B. Transformation-Optics Description of Plasmonic Nanostructures Containing Blunt Edges/Corners: From Symmetric to Asymmetric Edge Rounding. *ACS Nano* **2012**, *6*, 6492−6506.

(17) Vercruysse, D.; Sonnefraud, Y.; Verellen, N.; Fuchs, F. B.; Di Martino, G.; Lagae, L.; Moshchalkov, V. V.; Maier, S. A.; Van Dorpe, P. Unidirectional Side Scattering of Light by a Single-Element Nanoantenna. *Nano Lett.* **2013**, *13*, 3843−3849.

(18) Mirin, N. A.; Ali, T. A.; Nordlander, P.; Halas, N. J. Perforated Semishells: Far-Field Directional Control and Optical Frequency Magnetic Response. *ACS Nano* **2010**, *4*, 2701−2712.

(19) Meng, X. G.; Guler, U.; Kildishev, A. V.; Fujita, K.; Tanaka, K.; Shalaev, V. M. Unidirectional Spaser in Symmetry-Broken Plasmonic Core-Shell Nanocavity. *Sci. Rep.* **2013**, *3*, 1241.

(20) Rodriguez-Fortuno, F. J.; Marino, G.; Ginzburg, P.; O'Connor, D.; Martinez, A.; Wurtz, G. A.; Zayats, A. V. Near-Field Interference for the Unidirectional Excitation of Electromagnetic Guided Modes. *Science* **2013**, *340*, 328−330.

(21) Liu, T. R.; Shen, Y.; Shin, W.; Zhu, Q. Z.; Fan, S. H.; Jin, C. J. Dislocated Double-Layer Metal Gratings: An Efficient Unidirectional Coupler. *Nano Lett.* **2014**, *14*, 3848−3854.

(22) Lopez-Tejeira, F.; Rodrigo, S. G.; Martin-Moreno, L.; Garcia-Vidal, F. J.; Devaux, E.; Ebbesen, T. W.; Krenn, J. R.; Radko, I. P.;

Bozhevolnyi, S. I.; Gonzalez, M. U.; Weeber, J. C.; Dereux, A. Efficient unidirectional nanoslit couplers for surface plasmons. *Nat. Phys.* **2007**, *3*, 324−328.

(23) Lu, F.; Sun, L.; Wang, J.; Li, K.; Xu, A. S. Broad-angle and efficient unidirectional excitations of surface plasmons with dielectric-coated subwavelength metallic periodic nanoslits. *Appl. Phys. Lett.* **2014**, *105*, 091112.

(24) Liu, Y. M.; Palomba, S.; Park, Y.; Zentgraf, T.; Yin, X. B.; Zhang, X. Compact Magnetic Antennas for Directional Excitation of Surface Plasmons. *Nano Lett.* **2012**, *12*, 4853−4858.

(25) Chen, J. J.; Li, Z.; Lei, M.; Yue, S.; Xiao, J. H.; Gong, Q. H. Broadband unidirectional generation of surface plasmon polaritons with dielectric-film-coated asymmetric single-slit. *Opt. Express* **2011**, *19*, 26463−26469.

(26) Raether, H. *Surface Plasmons on Smooth and Rough Surfaces and on Gratings*; Springer-Verlag: Berlin, 1988.

(27) Lin, J.; Mueller, J. P. B.; Wang, Q.; Yuan, G. H.; Antoniou, N.; Yuan, X. C.; Capasso, F. Polarization-Controlled Tunable Directional Coupling of Surface Plasmon Polaritons. *Science* **2013**, *340*, 331−334.

(28) Huang, X. P.; Brongersma, M. L. Compact Aperiodic Metallic Groove Arrays for Unidirectional Launching of Surface Plasmons. *Nano Lett.* **2013**, *13*, 5420−5424.

(29) Li, G. Y.; Zhang, J. S. Ultra-broadband and efficient surface plasmon polariton launching through metallic nanoslits of subwavelength period. *Sci. Rep.* **2014**, *4*, 5914.

(30) Bao, Y. J.; Zu, S.; Zhang, Y. F.; Fang, Z. Y. Active Control of Graphene-Based Unidirectional Surface Plasmon Launcher. *ACS Photonics* **2015**, *2*, 1135−1140.

(31) Johnson, P. B.; Christy, R. W. Optical Constants of the Noble Metals. *Phys. Rev. B* **1972**, *6*, 4370−4379.

(32) Baida, F. I.; Belkhir, A.; Van Labeke, D.; Lamrous, O. Subwavelength metallic coaxial waveguides in the optical range: Role of the plasmonic modes. *Phys. Rev. B: Condens. Matter Mater. Phys.* **2006**, *74*, 205419.

(33) van Beijnum, F.; Retif, C.; Smiet, C. B.; Liu, H. T.; Lalanne, P.; van Exter, M. P. Quasi-cylindrical wave contribution in experiments on extraordinary optical transmission. *Nature* **2012**, *492*, 411−414.

(34) Liu, H. T.; Lalanne, P. Microscopic theory of the extraordinary optical transmission. *Nature* **2008**, *452*, 728−731.

(35) Haftel, M. I.; Schlockermann, C.; Blumberg, G. Enhanced transmission with coaxial nanoapertures: Role of cylindrical surface plasmons. *Phys. Rev. B: Condens. Matter Mater. Phys.* **2006**, *74*, 235405.

(36) Ni, H. B.; Wang, M.; Shen, T. Y.; Zhou, J. Self-Assembled Large-Area Annular Cavity Arrays with Tunable Cylindrical Surface Plasmons for Sensing. *ACS Nano* **2015**, *9*, 1913−1925.